

Fluctuating charge-density waves in the Hubbard model

Alexei Sherman

Institute of Physics, University of Tartu, Riia 142, 51014 Tartu, Estonia

Michael Schreiber

Institut für Physik, Technische Universität, 09107 Chemnitz, Germany

(Received 10 January 2008; revised manuscript received 7 March 2008; published 17 April 2008)

The charge susceptibility of the two-dimensional repulsive Hubbard model is investigated by using the diagram technique developed for the case of strong correlations. In this technique, a power series in the hopping constant is used. It is shown that once the Fermi level crosses one of the Hubbard subbands, a sharp peak appears in the momentum dependence of the static susceptibility. With further departure from half-filling, the peak transforms to a ridge around the Γ point. Within the considered range $0 \leq |1 - \bar{n}| \leq 0.2$ of the electron filling \bar{n} , the static susceptibility is finite, which points to the absence of long-range charge ordering. However, for $|1 - \bar{n}| \approx 0.12$, the susceptibility maxima are located halfway between the center and the boundaries of the Brillouin zone. In this case, an interaction of the carriers with the tetragonal distortions can stabilize the charge-density wave with the wavelength of four lattice spacings, as experimentally observed in the low-temperature tetragonal phase of lanthanum cuprates. Within the range of parameters inherent in cuprate perovskites, the character of the susceptibility evolution with \bar{n} depends only weakly on the ratio of the nearest-neighbor hopping constant to the Hubbard repulsion and on details of the initial band structure. The location of the susceptibility maxima in the Brillouin zone is mainly determined by the value of \bar{n} .

DOI: [10.1103/PhysRevB.77.155117](https://doi.org/10.1103/PhysRevB.77.155117)

PACS number(s): 71.10.Fd, 71.27.+a, 71.45.Lr, 74.25.Kc

I. INTRODUCTION

A variety of numerical methods have been used to elucidate the existence of phase separation in the ground states of the Hubbard and the related t - J models. States with charge-density waves (CDWs) (stripes) were obtained in Refs. 1–6 by using the mean-field approximation, the variational principle with the Gutzwiller-type variational functions, and the density matrix renormalization group calculations. However, the results of the Monte Carlo simulations^{7–9} and cluster calculations^{10,11} cast doubt on this finding. Hence, different techniques give different results, which reflect the fact that nearly degenerate low-lying states of the models have different natures.

Experimentally static stripes were observed^{12–15} in the low-temperature tetragonal (LTT) phase of lanthanum cuprates, $\text{La}_{1.6-x}\text{Nd}_{0.4}\text{Sr}_x\text{CuO}_4$ and $\text{La}_{2-x}\text{Ba}_x\text{CuO}_4$. One of the manifestations of the stripe formation is the anomalous suppression of superconductivity near the hole concentration $x = 1/8$ in $\text{La}_{2-x}\text{Ba}_x\text{CuO}_4$. A weaker suppression of T_c near this hole concentration is also observed in $\text{La}_{2-x}\text{Sr}_x\text{CuO}_4$ in the low-temperature orthorhombic (LTO) phase.¹⁶ The mentioned phases are characterized by tilts of the CuO_6 octahedrons about the axes (LTT) and the diagonals (LTO) of the Cu-O planes. These experimental observations suggest that the interaction of the carriers with the respective phonons plays an essential role in the stripe stabilization.

For investigating the instabilities of a system, it is convenient to use the corresponding static susceptibilities. Similar to the divergence of magnetic susceptibility, which points to the establishment of long-range magnetic order while finite maxima indicate short-range ordering, a divergence of charge susceptibility means the appearance of a CDW, while the finite peaks are manifestations of the respective charge fluctuations. In this paper, we calculate the charge suscepti-

bility of the two-dimensional repulsive Hubbard model by using the strong-coupling diagram technique. In this technique,^{17–20} on the assumption of strong electron correlations, Green's functions are calculated by using an expansion in powers of the hopping constant. The terms of this expansion are expressed by means of site cumulants of electron creation and annihilation operators.

It is found that once the Fermi level crosses one of the Hubbard subbands, a sharp maximum appears in the momentum dependence of the static susceptibility near the Γ point. With further departure of the electron filling \bar{n} from the half-filling value $\bar{n} = 1$, the maximum transforms into a ridge around the Γ point. Within the considered range of the electron filling $0 \leq |1 - \bar{n}| \leq 0.2$, the static susceptibility is finite, which implies the absence of long-range charge ordering. However, the obtained results give some insight into the way in which phonons can stabilize stripes. For $|1 - \bar{n}| \approx 0.12$, the susceptibility maxima are located halfway between the center and the boundaries of the Brillouin zone. In this case, an interaction of the carriers with the tetragonal distortions gives a maximal energy gain for the CDW with a wavelength of four lattice spacings, as experimentally observed in the LTT phase of lanthanum cuprates. The calculations were carried out for the t - t' - U Hubbard model for the ratios of the Hubbard repulsion to the nearest-neighbor hopping constant $U/|t| = 8$ and 12 and for the next-nearest-neighbor hopping constant $t' = 0$ and $-0.3t$. The above-discussed evolution of the susceptibility with \bar{n} is not qualitatively changed with variations in U/t and t'/t . The shape of the susceptibility and the location of its maxima in the Brillouin zone are mainly determined by the value of \bar{n} . The mentioned values of the parameters belong to the parameter range that is widely believed to be suitable for cuprate perovskites.

The main formulas that are used in the calculations are given in Sec. II. The discussion of the obtained results and

their comparison with the Monte Carlo simulations are carried out in Sec. III. Concluding remarks are presented in Sec. IV.

II. MAIN FORMULAS

The Hubbard model is described by the Hamiltonian,

$$H = \sum_{\mathbf{l}\mathbf{l}'\sigma} t_{\mathbf{l}\mathbf{l}'} a_{\mathbf{l}\sigma}^\dagger a_{\mathbf{l}'\sigma} + \frac{U}{2} \sum_{\mathbf{l}\sigma} n_{\mathbf{l}\sigma} n_{\mathbf{l},-\sigma}, \quad (1)$$

where $a_{\mathbf{l}\sigma}^\dagger$ and $a_{\mathbf{l}\sigma}$ are the electron creation and annihilation operators, \mathbf{l} labels sites of the square plane lattice, $\sigma = \uparrow$ or \downarrow is the spin projection, $t_{\mathbf{l}\mathbf{l}'}$ and U are hopping and on-site repulsion constants, and $n_{\mathbf{l}\sigma} = a_{\mathbf{l}\sigma}^\dagger a_{\mathbf{l}\sigma}$. Below, we consider the case wherein only the nearest-neighbor t and next-nearest-neighbor t' hopping constants are nonzero.

As mentioned above, in the considered case of strong correlations, $U \gg |t|$, t' , we use the strong-coupling diagram technique¹⁷⁻²⁰ for calculating the charge Green's function,

$$B_{\sigma'\sigma}(\mathbf{l}'\tau', \mathbf{l}\tau) = \langle T \delta n_{\mathbf{l}'\sigma'}(\tau') \delta n_{\mathbf{l}\sigma}(\tau) \rangle, \quad (2)$$

where $\delta n_{\mathbf{l}\sigma} = n_{\mathbf{l}\sigma} - \langle n_{\mathbf{l}\sigma} \rangle$ is the deviation of the electron occupation number from its mean value, the angular brackets denote the statistical averaging with the Hamiltonian,

$$\mathcal{H} = H - \mu \sum_{\mathbf{l}\sigma} n_{\mathbf{l}\sigma},$$

where μ is the chemical potential and T is the time-ordering operator that arranges other operators from right to left in ascending order of times τ . The time evolution of operators in Eq. (2) is also determined by the Hamiltonian \mathcal{H} ,

$$O(\tau) = \exp(\mathcal{H}\tau) O \exp(-\mathcal{H}\tau).$$

By using the strong-coupling diagram technique, one can convince oneself that equations for B are similar to those derived for the spin Green's function in Ref. 21. After the Fourier transformation, these equations read

$$\begin{aligned} B_{\sigma'\sigma}(q) = & -\delta_{\sigma'\sigma} \frac{T}{N} \sum_{p_1} G(p_1) G(q+p_1) \\ & + \left(\frac{T}{N}\right)^2 \sum_{p_1 p_2} \Pi(p_1) \Pi(p_2) \Pi(q+p_1) \\ & \times \Pi(q+p_2) \Lambda_{\sigma'\sigma}(p_1, q+p_1, q+p_2, p_2), \quad (3) \end{aligned}$$

$$\begin{aligned} \Lambda_{\sigma'\sigma}(p_1, q+p_1, q+p_2, p_2) = & \lambda_{\sigma'\sigma}(p_1, q+p_1, q+p_2, p_2) \\ & - \frac{T}{N} \sum_{p_3 \sigma_1} \lambda_{\sigma'\sigma_1}(p_1, q+p_1, q \\ & + p_3, p_3) \Theta(p_3) \Theta(q+p_3) \\ & \times \Lambda_{\sigma_1\sigma}(p_3, q+p_3, q+p_2, p_2). \quad (4) \end{aligned}$$

Here, the combined indices $q = (\mathbf{k}, i\omega_q)$ and $p_j = (\mathbf{k}_j, i\omega_{p_j})$ are introduced, $\omega_p = 2\nu\pi T$ and $\omega_n = (2n+1)\pi T$ are the boson and

fermion Matsubara frequencies with temperature T , \mathbf{k} is the wave vector, $G(p) = \langle \langle a_{\mathbf{k}\sigma} | a_{\mathbf{k}\sigma}^\dagger \rangle \rangle$ is the electron Green's function, $\Pi(p) = 1 + t_{\mathbf{k}} G(p)$, $t_{\mathbf{k}}$ is the Fourier transform of the hopping constants, which is equal to $t_{\mathbf{k}} = 2t[\cos(k_x) + \cos(k_y)] + 4t' \cos(k_x)\cos(k_y)$ in the considered case, the lattice spacing is taken as the unit of length, $\Theta(p) = t_{\mathbf{k}} \Pi(p)$ is the renormalized hopping, $\Lambda_{\sigma'\sigma}(p_1, p+p_1, p+p_2, p_2)$ is the sum of all of the four-leg diagrams, $\lambda_{\sigma'\sigma}(p_1, p+p_1, p+p_2, p_2)$ is its irreducible subset, and N is the number of sites.

The main difference between Eqs. (3) and (4) and the respective equations for the spin Green's function²¹ is in the spin indices of the irreducible four-leg diagrams. For the transversal spin Green's function that was considered in Ref. 21, only $\lambda_{\uparrow\downarrow}(p_1, p+p_1, p+p_2, p_2)$ enters into the equations.

Equations (3) and (4) can be somewhat simplified if we take into account the invariance of Hamiltonian (1) with respect to the rotations of the spin quantization axis.²² This invariance leads to symmetry relations,

$$B_{\uparrow\uparrow}(q) = B_{\downarrow\downarrow}(q), \quad B_{\uparrow\downarrow}(q) = B_{\downarrow\uparrow}(q),$$

and analogously for $\Lambda_{\sigma'\sigma}$ and $\lambda_{\sigma'\sigma}$. By using these relations, we find the following from Eqs. (3) and (4):

$$\begin{aligned} B(q) = & -\frac{T}{N} \sum_{p_1} G(p_1) G(q+p_1) + \left(\frac{T}{N}\right)^2 \sum_{p_1 p_2} \Pi(p_1) \Pi(p_2) \\ & \times \Pi(q+p_1) \Pi(q+p_2) \Lambda(p_1, q+p_1, q+p_2, p_2), \quad (5) \end{aligned}$$

$$\begin{aligned} \Lambda(p_1, q+p_1, q+p_2, p_2) = & \lambda(p_1, q+p_1, q+p_2, p_2) \\ & - \frac{T}{N} \sum_{p_3} \lambda(p_1, q+p_1, q+p_3, p_3) \\ & \times \Theta(p_3) \Theta(q+p_3) \Lambda(p_3, q+p_3, q \\ & + p_2, p_2), \quad (6) \end{aligned}$$

where

$$B(q) = \frac{1}{2} \sum_{\sigma'\sigma} B_{\sigma'\sigma}(q),$$

$$\Lambda(p_1, q+p_1, q+p_2, p_2) = \frac{1}{2} \sum_{\sigma'\sigma} \Lambda_{\sigma'\sigma}(p_1, q+p_1, q+p_2, p_2),$$

$$\lambda(p_1, q+p_1, q+p_2, p_2) = \frac{1}{2} \sum_{\sigma'\sigma} \lambda_{\sigma'\sigma}(p_1, q+p_1, q+p_2, p_2). \quad (7)$$

Diagrams corresponding to Eqs. (5) and (6) are plotted in Fig. 1. In these diagrams, the dual line indicates the electron Green's function $G(p)$, the shaded and open squares stand for Λ and λ , respectively, the single directed line between the squares is the renormalized hopping $\Theta(p)$, and the dashed line is the external line of the four-leg diagram with the

inserted irreducible two-leg diagrams. The dashed line corresponds to $\Pi(p)$.

In the following consideration, we simplify the general equations (5) and (6) by neglecting the irreducible two-leg diagrams in the external and internal lines of the four-leg diagrams. In these approximation quantities, $\Pi(p)$ and $\Theta(p)$ in Eqs. (5) and (6) are substituted by 1 and $t_{\mathbf{k}}$, respectively. Besides, we use the lowest-order irreducible four-leg diagram instead of $\lambda_{\sigma'\sigma}(p_1, q+p_1, q+p_2, p_2)$. This four-leg diagram is described by the second-order cumulant of electron operators,

$$\begin{aligned} K_2^{\sigma'\sigma}(\tau', \tau, \tau'_1, \tau_1) &= \langle T \bar{a}_{\sigma'}(\tau') a_{\sigma'}(\tau) \bar{a}_{\sigma}(\tau'_1) a_{\sigma}(\tau_1) \rangle_0 \\ &\quad - K_1(\tau', \tau) K_1(\tau'_1, \tau_1) \\ &\quad + K_1(\tau', \tau_1) K_1(\tau'_1, \tau) \delta_{\sigma'\sigma}, \end{aligned} \quad (8)$$

where the subscript 0 of the angular brackets indicates that the averaging and time dependencies of operators are determined by the site Hamiltonian,

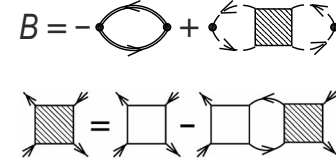


FIG. 1. Diagrams corresponding to Eqs. (5) and (6).

$$H_1 = \sum_{\sigma} [(U/2)n_{1\sigma}n_{1,-\sigma} - \mu n_{1\sigma}], \quad (9)$$

$\bar{a}_{1\sigma}(\tau) = \exp(H_1\tau) a_{1\sigma}^{\dagger} \exp(-H_1\tau)$ and the first-order cumulant $K_1(\tau', \tau) = \langle T \bar{a}_{\sigma}(\tau') a_{\sigma}(\tau) \rangle_0$. This cumulant does not depend on the spin index σ and the respective superscript is dropped in the cumulant notation. All operators in the cumulants belong to the same lattice site. Due to the translational symmetry of the problem, the cumulants do not depend on the site index, which is therefore omitted in the above equations. After the Fourier transformation, the expression for $K_2^{\sigma'\sigma}$ reads

$$\begin{aligned} K_2^{\sigma'\sigma}(n_1, \nu + n_1, \nu + n_2, n_2) &= Z^{-1} \{ \beta [(\delta_{\nu 0} \delta_{\sigma'\sigma} - \delta_{n_1 n_2}) e^{-E_1 \beta} + Z^{-1} (\delta_{\nu 0} - \delta_{n_1 n_2} \delta_{\sigma'\sigma}) (e^{-(E_0 + E_2) \beta} - e^{-2E_1 \beta})] F(n_1 + \nu) F(n_2) \\ &\quad - \delta_{\sigma', -\sigma} e^{-E_0 \beta} U g_{01}(n_1 + \nu) g_{01}(n_2) g_{02}(n_1 + n_2 + \nu) [g_{01}(n_2 + \nu) + g_{01}(n_1)] - \delta_{\sigma', -\sigma} e^{-E_2 \beta} U g_{12}(n_1 \\ &\quad + \nu) g_{12}(n_2) g_{02}(n_1 + n_2 + \nu) [g_{12}(n_2 + \nu) + g_{12}(n_1)] + \delta_{\sigma', -\sigma} e^{-E_1 \beta} [F(n_1 + \nu) g_{01}(n_2) g_{01}(n_2 + \nu) \\ &\quad + F(n_2) g_{01}(n_1 + \nu) g_{01}(n_1) + F(n_2) g_{12}(n_2 + \nu) [g_{12}(n_1 + \nu) - g_{01}(n_1)] + F(n_1 + \nu) g_{12}(n_1) [g_{12}(n_2) \\ &\quad - g_{01}(n_2 + \nu)] \}, \end{aligned} \quad (10)$$

where $E_0 = 0$, $E_1 = -\mu$, and $E_2 = U - 2\mu$ are the eigenenergies of site Hamiltonian (9), $\beta = T^{-1}$, $Z = e^{-E_0 \beta} + 2e^{-E_1 \beta} + e^{-E_2 \beta}$ is the site partition function, $g_{ij}(n) = (i\omega_n + E_i - E_j)^{-1}$, and $F(n) = g_{01}(n) - g_{12}(n)$, and the integers n and ν stand for the fermion and the boson Matsubara frequencies.

Equation (10) can be significantly simplified for the case of principal interest $U \gg T$. In this case, if μ satisfies the condition,

$$\eta < \mu < U - \eta, \quad (11)$$

where $\eta \gg T$, the exponent $e^{-\beta E_1}$ is much larger than $e^{-\beta E_0}$ and $e^{-\beta E_2}$. Therefore, the terms with $e^{-\beta E_0}$ and $e^{-\beta E_2}$ can be omitted in Eq. (10). In this case, we obtain the following for the quantity of $K_2 = 1/2 \sum_{\sigma'\sigma} K_2^{\sigma'\sigma}$, which is used instead of λ in Eq. (6):

$$\begin{aligned} K_2(n_1, \nu + n_1, \nu + n_2, n_2) &= -\frac{3}{4} \beta \delta_{n_1 n_2} F(n_1 + \nu) F(n_2) + \frac{1}{2} \{ F(n_1 + \nu) g_{01}(n_2) g_{01}(n_2 + \nu) + F(n_2) g_{01}(n_1 + \nu) g_{01}(n_1) \\ &\quad + F(n_2) g_{12}(n_2 + \nu) [g_{12}(n_1 + \nu) - g_{01}(n_1)] + F(n_1 + \nu) g_{12}(n_1) [g_{12}(n_2) - g_{01}(n_2 + \nu)] \}. \end{aligned} \quad (12)$$

As can be seen from Eq. (6), in this approximation, $\Lambda(\mathbf{k}_1, \omega_{n_1}; \mathbf{k} + \mathbf{k}_1, \omega_{\nu} + \omega_{n_1}; \mathbf{k} + \mathbf{k}_2, \omega_{\nu} + \omega_{n_2}; \mathbf{k}_2, \omega_{n_2})$ does not depend on \mathbf{k}_1 and \mathbf{k}_2 .

Taking into account these simplifications, we find for the second term on the right-hand side of Eq. (5)

$$\begin{aligned} \left(\frac{T}{N} \right)^2 \sum_{p_1 p_2} \Lambda &= -\frac{3}{4} T \sum_n f_{\mathbf{k}}(\nu n) a_1(\nu + n) a_1(n) - \frac{1}{2} [1 + S_{\mathbf{k}} \gamma_4(\mathbf{k}\nu)] T \sum_n f_{\mathbf{k}}(\nu n) a_3(-\nu, \nu + n) \\ &\quad + \frac{1}{2} [1 - S_{\mathbf{k}} \gamma_1(\mathbf{k}\nu)] T \sum_n f_{\mathbf{k}}(\nu n) a_2(-\nu, \nu + n) + \frac{1}{2} \left[\frac{1}{i\omega_{\nu} - U} - S_{\mathbf{k}} \gamma_3(\mathbf{k}\nu) \right] T \sum_n f_{\mathbf{k}}(\nu n) a_4(-\nu, \nu + n) \\ &\quad - \frac{1}{2} S_{\mathbf{k}} \gamma_2(\mathbf{k}\nu) T \sum_n f_{\mathbf{k}}(\nu n) a_1(\nu + n), \end{aligned} \quad (13)$$

where

$$\begin{aligned}
S_{\mathbf{k}} &= N^{-1} \sum_{\mathbf{k}'} t_{\mathbf{k}+\mathbf{k}'} t_{\mathbf{k}'}, \\
f_{\mathbf{k}}(v n) &= \left[1 - \frac{3}{4} S_{\mathbf{k}} F(v+n) F(n) \right]^{-1}, \\
a_1(n) &= F(n), \quad a_2(v n) = g_{01}(n) g_{01}(v+n), \\
a_3(v n) &= F(n) g_{12}(v+n), \\
a_4(v n) &= g_{12}(n) - g_{01}(v+n),
\end{aligned} \tag{14}$$

and $y_i(\mathbf{k} \nu)$ are solutions of the following system of four linear equations:

$$\begin{aligned}
y_i(\mathbf{k} \nu) &= T^2 \sum_{n_1 n_2} f_{\mathbf{k}}(v n_1) K_2(n_1, v+n_1, v+n_2, n_2) a_i(v n_1) \\
&- \frac{1}{2} S_{\mathbf{k}} T \sum_n f_{\mathbf{k}}(v n) a_1(v+n) a_i(v n) y_2(\mathbf{k} \nu) \\
&- \frac{1}{2} S_{\mathbf{k}} T \sum_n f_{\mathbf{k}}(v n) a_2(-v, v+n) a_i(v n) y_1(\mathbf{k} \nu) \\
&- \frac{1}{2} S_{\mathbf{k}} T \sum_n f_{\mathbf{k}}(v n) a_4(-v, v+n) a_i(v n) y_3(\mathbf{k} \nu) \\
&- \frac{1}{2} S_{\mathbf{k}} T \sum_n f_{\mathbf{k}}(v n) a_3(-v, v+n) a_i(v n) y_4(\mathbf{k} \nu).
\end{aligned} \tag{15}$$

The system of Eq. (15) follows from Eq. (6),

$$y_i(\mathbf{k} \nu) = T^2 \sum_{n_1 n_2} a_i(v n_1) \Lambda_{\mathbf{k}}(n_1, v+n_1, v+n_2, n_2).$$

In calculating the first term on the right-hand side of Eq. (5), we use the Hubbard-I approximation²³ for the electron Green's function. Under condition (11), this function reads

$$G(\mathbf{k} n) = \frac{i\omega_n + \mu - U/2}{(i\omega_n + \mu)(i\omega_n + \mu - U) - t_{\mathbf{k}}(i\omega_n + \mu - U/2)}. \tag{16}$$

III. CHARGE SUSCEPTIBILITY

In this section, we consider the static charge susceptibility,

$$\chi_c(\mathbf{k}) = B(\mathbf{k}, \nu=0).$$

As mentioned above, divergence of this quantity points to a charge instability of the system, while its finite maxima indicate the regions of increased charge response on an external field. To check the used approximation, we compare our results that were obtained for a 4×4 lattice to the data of the Monte Carlo simulations carried out for the same conditions.²⁴ This comparison is demonstrated in Fig. 2. In Fig. 2, $\bar{n} = \sum_{\sigma} \langle n_{1\sigma} \rangle$ is the electron filling. The value $\bar{n}=1$ corresponds to half-filling. We used a small global vertical shift

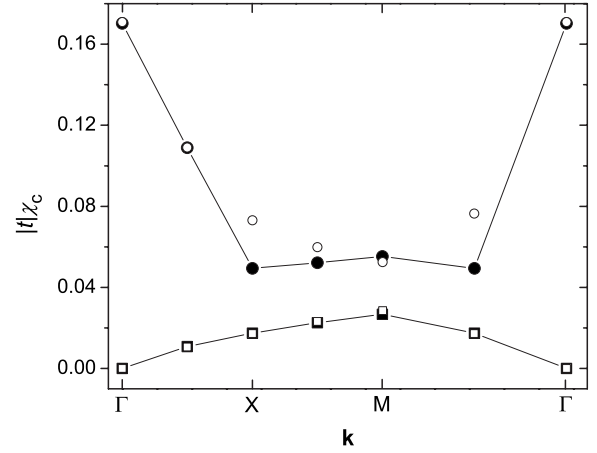


FIG. 2. The static charge susceptibility in a 4×4 lattice for $t = -U/8$, $t' = 0$, and $T = 0.125|t|$. The susceptibility is plotted along the triangular contour in the Brillouin zone. The corners of the contour are given by the momenta $\mathbf{k} = (0, 0)$ (Γ), $(\pi, 0)$ (X), and (π, π) (M). The open symbols are the results of the Monte Carlo simulations (Ref. 24) for $\bar{n}=1$ (squares) and $\bar{n}=0.95$ (circles). The filled symbols are our results for the same electron fillings.

in our results to better fit the Monte Carlo data. As seen from Fig. 2, our approximation correctly reproduces the general shape of the dependence $\chi_c(\mathbf{k})$ and its variation with electron filling. Notice the rapid increase in the uniform susceptibility $\chi_c(\mathbf{0})$ with departure from half-filling.

The susceptibility for a larger lattice and a smaller temperature is shown in Fig. 3. At half-filling, the susceptibility is small and its dependence on momentum is weak, as can be seen in Fig. 3(a). This shape of $\chi_c(\mathbf{k})$ is retained until the Fermi level crosses one of the Hubbard subbands. Immediately after this crossing, which leads to a departure from half-filling, a sharp peak appears in the dependence $\chi_c(\mathbf{k})$. As shown in Fig. 3(b), the peak is finite and is located near the Γ point, which indicates the appearance of a long-wave charge fluctuation in the system. With increasing $x = |1 - \bar{n}|$, the susceptibility grows. For moderate values of x , it peaks for momenta along a contour that is centered on the Γ point and has the shape of a somewhat distorted circle [see Fig. 3(c)]. With the increase in x , the size of the contour grows, indicating a decrease in the wavelength of charge fluctuations. Notice that in Fig. 3(c), for $x \approx 0.12$, the contour crosses the axes at $k_x, k_y \approx \pi/2$. On approaching the boundary of the considered range of μ [Eq. (11)], the susceptibility starts to grow near the X and Y [$(0, \pi)$] points [see Fig. 3(d)]. For chemical potentials within this range, the contour does not cross the boundary of the magnetic Brillouin zone—the line segment connecting the X and Y points. Notice also that within this range corresponding to electron fillings of $0 \leq x \leq 0.2$, which are most interesting for cuprate perovskites, the susceptibility remains finite. This means that a long-range or stripe ordering of charges *does not occur* in the Hubbard model for the considered parameters. The model produces only charge fluctuations with wave vectors corresponding to the maxima of the susceptibility. The susceptibility varies only slightly with a further decrease in temperature from the value used in Fig. 3.

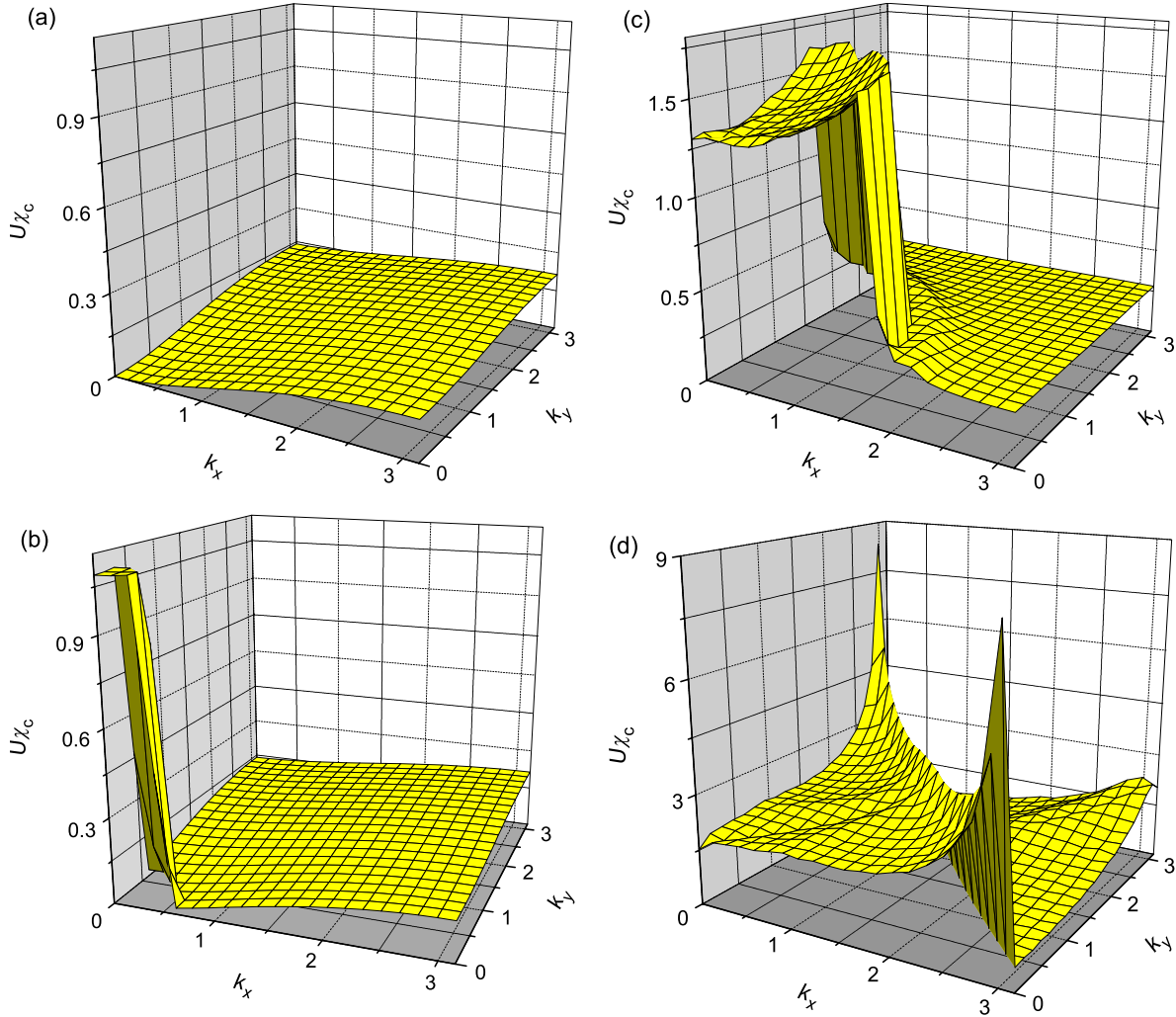


FIG. 3. (Color online) The static charge susceptibility in a 40×40 lattice for $t = -U/8$, $t' = 0$, and $T = 0.001U$. The susceptibility is shown in the first quadrant of the Brillouin zone for the electron fillings (a) $\bar{n} = 1$, (b) 0.97, (c) 0.88, and (d) 0.8.

The results shown in Fig. 3 were obtained for the t - U Hubbard model with the ratio of parameters $U/|t| = 8$. To check how this overall picture is changed with the variation in the parameters, we carried out analogous calculations for the t - U model with $U/|t| = 12$ and for the t - t' - U model with $U/|t| = 8$ and $t' = -0.3t$. This latter ratio of the hopping constants is believed to adequately describe the band structure of cuprate perovskites.²⁵ In both cases, the evolution with filling and the shape of the susceptibility qualitatively look the same as those shown in Fig. 3. Moreover, the location of the susceptibility maxima in the Brillouin zone varies only slightly with the change in the hopping and repulsion constants and is mainly determined by the electron filling. As an example, the susceptibilities for the two considered sets of parameters are shown in Fig. 4 for $\bar{n} \approx 0.88$. These susceptibilities should be compared to Fig. 3(c). Notice that, as in Fig. 3(c), the maxima on the axes of the Brillouin zone are located approximately halfway between its center and boundary. It is also worth noting that in the t - t' - U model, which does not possess electron-hole symmetry, the shapes of the susceptibility are qualitatively similar for the fillings $\bar{n} = 1 - x$ and $1 + x$.

The appearance of maxima in the susceptibility with departure from half-filling is connected with the fermion poles of the function Λ , specifically with the poles given by the function $f_{\mathbf{k}}(\nu n)$ in Eq. (14). In general, these poles do not coincide with the poles of the electron Green's function $G(p)$. For $\nu = 0$, we find four poles of the function $f_{\mathbf{k}}(\nu = 0, z)$ at frequencies

$$\varepsilon_i(\mathbf{k}) = -\mu + \frac{U}{2} \pm \sqrt{\frac{U^2}{4} \pm \sqrt{\frac{3}{4}} U^2 S_{\mathbf{k}}}. \quad (17)$$

After the transformation to real frequencies, sums over n in Eqs. (13) and (15) are transformed to sums over the above poles and the terms of these sums contain the multipliers $n_F[\varepsilon_i(\mathbf{k})]$, where $n_F(\omega) = [\exp(\beta\omega) + 1]^{-1}$ is the Fermi-Dirac distribution function. Thus, for low temperatures and a small to moderate departure from half-filling, these sums and the second term of $B(q)$ [Eq. (13)] will have a steplike shape as functions of momentum if one of the dispersions [Eq. (17)] crosses the Fermi level. This behavior is demonstrated in Figs. 3(b), 3(c), and 4.

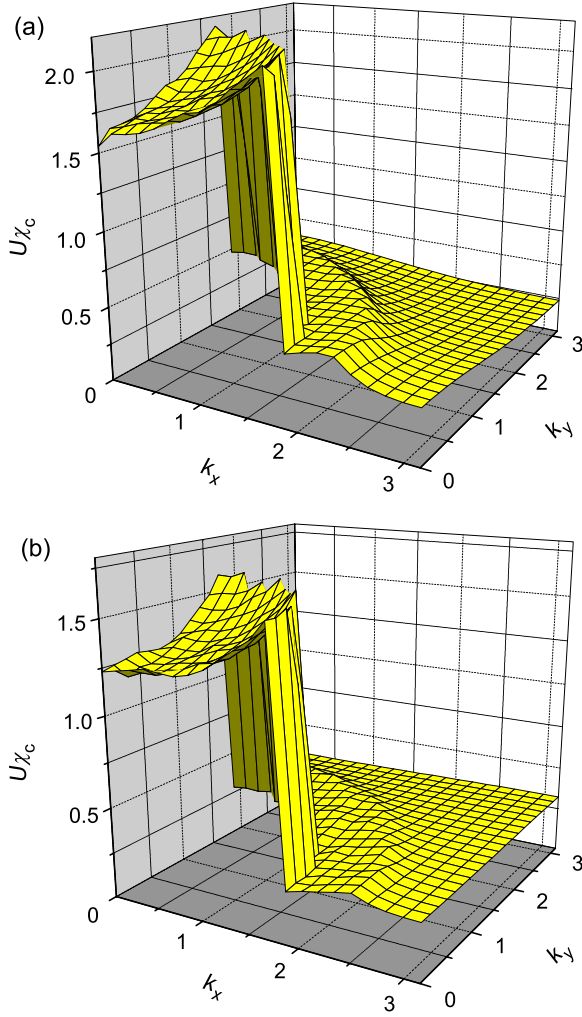


FIG. 4. (Color online) The static charge susceptibility in a 40×40 lattice (a) for $t = -U/12$, $t' = 0$ and (b) for $t = -U/8$, $t' = -0.3t$. In both cases, $\bar{n} \approx 0.88$ and $T = 0.001U$.

The above results do not support a purely electronic mechanism of long-range charge ordering. However, they give some insight into the way in which phonons can stabilize stripes. As mentioned above, an essential role of certain CuO_6 octahedron tilts in such stabilization can be supposed from experimental results^{12–15} on lanthanum cuprates. It is known^{26,27} that such tilts are strongly coupled to the carriers. This interaction can be described by using an effective electrostatic potential ϕ_1 that is connected with the charge fluctuations $\langle \delta n_1 \rangle$ arising in Cu-O planes as a consequence of the tilts. These fluctuations give the following contributions to the adiabatic potential:

$$\Delta E = -\frac{1}{2} \sum_{\mathbf{l}} \langle \delta n_{\mathbf{l}} \rangle \phi_{\mathbf{l}} = -\frac{1}{2} \sum_{\mathbf{k}} \chi_c(\mathbf{k}) \phi_{\mathbf{k}}^2. \quad (18)$$

Here, we took into account that the charge susceptibility is the response of the system on the external potential. In Eq. (18), we also allowed for the low frequency of the octahedron tilts.²⁶ The potential $\phi_{\mathbf{k}}$ depends on the coordinates Q_{k_x} , Q_{k_y} of these vibrations. Due to the symmetry of the problem,

with respect to a reflection in a Cu-O plane, this dependence contains only even powers of the coordinates and starts from quadratic terms,

$$\phi_{\mathbf{k}} = A_{\mathbf{k}} Q_{k_x}^2 + B_{\mathbf{k}} Q_{k_y}^2 + C_{\mathbf{k}} Q_{k_x} Q_{k_y} + \dots \quad (19)$$

Hence, contribution (18) is a quartic function of the coordinates. As follows from Eqs. (18) and (19), finite values of the vibration coordinates give an energy gain, and the larger the value of the susceptibility is, the larger is the energy gain that can be achieved (the lattice stability is provided by other quartic and higher power terms of the adiabatic potential). For weak momentum dependencies of other parameters of the adiabatic potential, the largest energy gain is achieved for momenta at which the susceptibility is peaked. From symmetry considerations, it can be supposed that for the LTT distortions ($Q_{k_x} \neq 0, Q_{k_y} = 0$ and vice versa), this gain is achieved for maxima on the axes of the crystal plane and for the LTO distortions ($Q_{k_x} = \pm Q_{k_y}$) on its diagonals. Based on the experimental results,^{12–15} it is clear that for x within the range of 0.12 ± 0.02 and for temperatures $T \leq 50$ K (the domain of the LTT phase²⁸ in $\text{La}_{2-x}\text{Ba}_x\text{CuO}_4$), parameters of the adiabatic potential provide the lowest minimum for tetragonal distortions and outside this region for orthorhombic distortions. As can be seen in Figs. 3(c) and 4, for $x \approx 0.12$, the susceptibility maxima are located on the axes approximately halfway between the Γ and X , (Y) points. Such maxima give the lowest energy for the CDW with a wavelength equal to four lattice spacings, as experimentally observed in the LTT phase of lanthanum cuprates.^{12–15} Such a CDW is commensurate with the lattice, which is essential for its stability. On the contrary, for $x \approx 0.12$, an oblique CDW in the LTO phase is, in general, incommensurate [see Figs. 3(c) and 4], which can explain its more disordered character.¹⁵

Another conclusion that can be made from the analysis of experimental data^{14,15} and from the above results concerns the magnetic incommensurability observed^{29,30} in p -type cuprate perovskites in a wide range of hole concentrations, namely, that it is unlikely that the magnetic incommensurability is connected with charge stripes. In $\text{La}_{2-x}\text{Ba}_x\text{CuO}_4$, the LTT phase with stripes along Cu-O bonds exists in a narrow range of hole concentrations near $x = 0.12$.²⁸ Outside of this range, in LTO phase, stripes are more disordered¹⁵ and oblique. Based on the assumption that magnetic incommensurability is connected with the stripes, it is difficult to explain the location of the low-frequency incommensurate maxima in the magnetic susceptibility along the axes of the Brillouin zone in both phases and a smooth variation of the incommensurability parameter with doping through these phases. Mechanisms of the magnetic incommensurability in strongly correlated systems, which are not based on charge stripes, were considered in Refs. 21 and 31–33.

IV. CONCLUDING REMARKS

In this paper, we calculated the charge susceptibility of the two-dimensional repulsive t - t' - U Hubbard model by using the strong-coupling diagram technique. In this technique, on the assumption of strong electron correlations, Green's functions are calculated by using the expansion in powers of

the hopping constant. The terms of this expansion are expressed by means of site cumulants of electron creation and annihilation operators. For a small lattice, we found good agreement of the results that was obtained by this approach with the Monte Carlo simulations. In a larger lattice, it was found that once the Fermi level crosses one of the Hubbard subbands, a sharp peak appears in the momentum dependence of the static charge susceptibility near the Γ point. With further departure from half-filling, the peak transforms to a ridge around this point. These results were obtained for three sets of parameters: for the t - U model with ratios of the parameters $U/|t|=8$ and 12 and for the t - t' - U model with $U/|t|=8$ and $t'=-0.3t$. We found that the shapes of the susceptibility and the positions of its maxima are similar in all three cases and are mainly determined by the value of the electron filling \bar{n} . This suggests that the obtained shapes of the susceptibility are inherent in the parameter range of cuprate perovskites. Within the considered interval of the electron filling $0 \leq |1-\bar{n}| \leq 0.2$, the static susceptibility is finite, which points to the absence of long-range charge ordering.

However, obtained results give some insight into the way in which phonons can stabilize stripes. For $|1-\bar{n}| \approx 0.12$, the susceptibility maxima are located halfway between the center and the boundaries of the Brillouin zone. In this case, an interaction of the carriers with the tetragonal distortions gives a maximal energy gain for the charge-density wave that is oriented along the Cu-O bond and has a wavelength equal to four lattice spacings. Such stripes are observed in the low-temperature tetragonal phase of lanthanum cuprates. We also supposed that the obtained incommensurate location of the susceptibility maxima along the diagonals of the Brillouin zone can be the reason for the more disordered character of the oblique stripes in the low-temperature orthorhombic phase in comparison with the commensurate stripes of the low-temperature tetragonal phase.

ACKNOWLEDGMENT

This work was partially supported by the ETF under Grant No. 6918.

-
- ¹V. Hizhnyakov and E. Sigmund, *Physica C* **156**, 655 (1988).
²J. Zaanen and O. Gunnarsson, *Phys. Rev. B* **40**, 7391 (1989).
³K. Machida, *Physica C* **158**, 192 (1989).
⁴T. Giamarchi and C. Lhuillier, *Phys. Rev. B* **42**, 10641 (1990).
⁵G. An and J. M. J. van Leeuwen, *Phys. Rev. B* **44**, 9410 (1991).
⁶S. R. White and D. J. Scalapino, *Phys. Rev. Lett.* **81**, 3227 (1998).
⁷Y. M. Vil'k, L. Chen, and A.-M. S. Tremblay, *Phys. Rev. B* **49**, 13267 (1994).
⁸S. Sorella, G. B. Martins, F. Becca, C. Gazza, L. Capriotti, A. Parola, and E. Dagotto, *Phys. Rev. Lett.* **88**, 117002 (2002).
⁹V. I. Anisimov, M. A. Korotin, I. A. Nekrasov, Z. V. Pchelkina, and S. Sorella, *Phys. Rev. B* **66**, 100502(R) (2002).
¹⁰T. A. Maier, M. Jarrell, T. C. Schulthess, P. R. C. Kent, and J. B. White, *Phys. Rev. Lett.* **95**, 237001 (2005).
¹¹M. Aichhorn, E. Arrighoni, M. Potthoff, and W. Hanke, *Phys. Rev. B* **74**, 024508 (2006).
¹²J. M. Tranquada, B. J. Sternlieb, J. D. Axe, Y. Nakamura, and S. Uchida, *Nature (London)* **375**, 561 (1995).
¹³J. M. Tranquada, J. D. Axe, N. Ichikawa, Y. Nakamura, S. Uchida, and B. Nachumi, *Phys. Rev. B* **54**, 7489 (1996).
¹⁴M. Fujita, H. Goka, K. Yamada, and M. Matsuda, *Phys. Rev. Lett.* **88**, 167008 (2002).
¹⁵H. Kimura, Y. Noda, H. Goka, M. Fujita, K. Yamada, M. Mizumaki, N. Ikeda, and H. Ohsumi, *Phys. Rev. B* **70**, 134512 (2004).
¹⁶H. Takagi, T. Ido, S. Ishibashi, M. Uota, S. Uchida, and Y. Tokura, *Phys. Rev. B* **40**, 2254 (1989).
¹⁷M. I. Vladimirov and V. A. Moskalenko, *Teor. Mat. Fiz.* **82**, 428 (1990) [*Theor. Math. Phys.* **82**, 301 (1990)].
¹⁸W. Metzner, *Phys. Rev. B* **43**, 8549 (1991).
¹⁹S. Pairault, D. Sénéchal, and A.-M. S. Tremblay, *Eur. Phys. J. B* **16**, 85 (2000).
²⁰A. Sherman, *Phys. Rev. B* **73**, 155105 (2006); **74**, 035104 (2006).
²¹A. Sherman and M. Schreiber, *Phys. Rev. B* **76**, 245112 (2007).
²²E. Fradkin, *Field Theories of Condensed Matter Systems* (Addison-Wesley, New York, 1991).
²³J. C. Hubbard, *Proc. R. Soc. London, Ser. A* **276**, 238 (1963).
²⁴N. E. Bickers and D. J. Scalapino, arXiv:cond-mat/0010480 (unpublished).
²⁵M. M. Korshunov and S. G. Ovchinnikov, *Fiz. Tverd. Tela (Leningrad)* **43**, 399 (2001) [*Phys. Solid State* **43**, 416 (2001)]; A. Macridin, M. Jarrell, T. Maier, and G. A. Sawatzky, *Phys. Rev. B* **71**, 134527 (2005).
²⁶W. E. Pickett, R. E. Cohen, and H. Krakauer, *Phys. Rev. Lett.* **67**, 228 (1991).
²⁷S. Barišić and J. Zelenko, *Solid State Commun.* **74**, 367 (1990).
²⁸K. I. Kumagai, K. Kawano, I. Watanabe, K. Nishiyama, and K. Nagamine, *J. Supercond.* **7**, 63 (1994).
²⁹H. Yoshizawa, S. Mitsuda, H. Kitazawa, and K. Katsumata, *J. Phys. Soc. Jpn.* **57**, 3686 (1988).
³⁰R. J. Birgeneau, Y. Endoh, K. Kakurai, Y. Hidaka, T. Murakami, M. A. Kastner, T. R. Thurston, G. Shirane, and K. Yamada, *Phys. Rev. B* **39**, 2868 (1989).
³¹A.-M. S. Tremblay, B. Kyung, and D. Sénéchal, *Fiz. Nizk. Temp.* **32**, 561 (2006).
³²A. Sherman and M. Schreiber, *Phys. Rev. B* **69**, 100505(R) (2004); *Int. J. Mod. Phys. B* **19**, 2145 (2005); **21**, 669 (2007).
³³M. V. Eremin, A. A. Aleev, and I. M. Eremin, *Pis'ma Zh. Eksp. Teor. Fiz.* **84**, 197 (2006) [*JETP Lett.* **84**, 167 (2006)].